JOURNAL OF THERMOPHYSICS AND HEAT TRANSFER
Vol. 16, No. 2, April–June 2002

Examination of Water Dissociation Models in Shock Heated Air

Deborah A. Levin*
Pennsylvania State University, University Park, Pennsylvania 16802
Sergey F. Gimelshein†
George Washington University, Washington, D.C. 20052
and
Natalia E. Gimelshein‡
Pennsylvania State University, University Park, Pennsylvania 16802

A semiclassical molecular dynamics approach is used to model the dissociation of water to form the hydroxyl radical. The unimolecular dissociation of water is utilized to compute the probability of reaction, as well as to determine the product OH translational, vibrational, and rotational energy distributions. The flow regime of interest is that between 80 and 100 km, so that a rarefied gasdynamics technique must be used. The molecular dynamics probabilities of reactions and product distributions are, therefore, used in the direct simulation Monte Carlo method to model spatial distribution and temperatures of OH in the bow shock of a 5-km/s vehicle. The fraction of translational energy transferred to internal water energy during dissociative collisions was parameterized. The rates of OH production predicted by the molecular dynamics model are approximately a factor of five lower than those predicted by the total collisional energy model for 10% energy transfer and are approximately equal for 100% energy transfer.

Nomenclature

E_c	=	total collision energy
E_d	=	dissociation threshold
E_{int,H_2O}	=	internal (rotational and vibrational) energy of H_2O
E^T_{cm}	=	energy of the center of mass of H_2O
$E^{T_{\text{rel}}}_{H,OH}$	=	relative OH–H translational energy
E_{trn,H_2O-M}	=	relative translational energy of H_2O and M
H	=	Hamiltonian for the water molecule
J	=	rotational quantum number
m_i	=	mass of ith atom
p_{ij}	=	momentum of ith atom in jth direction
r_{ij}	=	coordinate of ith atom in jth direction
T	=	kinetic energy of water nuclei
V	=	potential energy of water
v	=	vibrational quantum number
Z_r	=	rotational relaxation number
Z_v	=	vibrational relaxation number
η	=	conversion efficiency of translational collision energy to internal water energy
ξ	=	number of degrees of freedom

Subscripts

int	=	internal
rot	=	rotational
trn	=	translational
vib	=	vibrational

Received 15 June 2001; revision received 16 October 2001; accepted for publication 17 October 2001.

*Associate Professor, Department of Aerospace Engineering, 233 Hammond Building. Senior Member AIAA.
†Senior Research Scientist, Department of Chemistry, 21st Street, North West.
‡Graduate Student, Department of Aerospace Engineering, 135 Hammond Building.

I. Introduction

THE modeling of chemical reactions in hypersonic flows requires the use of chemical rates and cross sections that are either obtained from experiments or derived theoretically. Most chemical rates are expressed in terms of an Arrhenius equation whose parameters are derived from shock tube studies often conducted at temperatures or thermal nonequilibrium conditions different from the flow conditions required in the modeling. Theoretical rate models generally are semi-empirical in nature, and it is difficult to quantify the errors made when they are applied to the general case. The availability of spectra of a hypersonic chemically reacting flow from the bow shock ultraviolet flight experiments[1] provided new impetus to improve the fidelity of chemical rates used in flowfield calculations. The work of Bose and Candler[2] showed that a quasi-classical trajectory method could be used to model the first Zeldovich reaction rate and that the populations of high vibrational levels of NO product is large compared to those of bulk N_2. In the work of Boyd et al.,[3] the molecular dynamics reaction cross sections were successfully used in the direct simulation Monte Carlo (DSMC) method. Application of the NO vibrational distributions has also been shown to be crucial for modeling high-altitude infrared spacecraft glow.[4] The ultraviolet NO spectra, however, is complicated by the contributions from multiple excited electronic states. In contrast, the UV spectra of OH is well defined and under rarefied conditions should be sensitive to the detailed processes involved in water dissociation in shock heated flows.

UV radiation from the OH ($A \rightarrow X$) system has been studied extensively in the combustion and atmospheric sciences communities.[5] The hydroxyl radical is also readily observed under various hypersonic flow conditions, where it is produced by shock chemistry reactions.[6] The strong spin-allowed transition from the first excited state, $A^2\Sigma^+$, to the ground state means that it is readily observable, even when present in trace quantities. Spectra of OH at altitudes of approximately 100 km were observed during the bow shock UV flight experiment 2 (BSUV2). The mission and instrumentation have been described previously.[1] Earlier work demonstrated the sensitivity of the OH spectra to variation in the vibrational temperature, and within the accuracy of the data the OH vibrational temperature was estimated to be between 4000 and 7000 K for 100 km (Ref. 7). Although this is a large temperature uncertainty, the OH vibrational temperature is significantly different than the predicted shock layer bulk (N_2) vibrational temperature of ~1000 K for this altitude.

To date, there has been no fundamental explanation of why the OH vibrational temperature in such flows is different from that of N_2. More detailed treatment of the coupling of the flow and radiation modeling has been undertaken for the OH(A) system.[8] This work, however, does not lead to OH vibrational temperatures consistent with the BSUV2. We have shown in previous work[1] that the dissociation of water primarily goes through collisions with N_2 at altitudes of 80 km. The freestream atmospheric constituents change between 80 and 100 km, and for flows at 100 km, the atomic oxygen may also be an important collider dissociating water. If we are to understand the mechanism for formation of vibrationally hot OH in transitional flows, we must expect to model in detail the fundamental processes of water collisionally induced excitation and dissociation by N_2 and O. Modeling of collisional excitation and reactions of polyatomic systems in high-temperature flows is a difficult problem. The efficiency of collisional energy transfer to the internal energy of the water molecule before dissociation will effect the OH product state distribution.

As a first step in this direction, the goal of this work is to present the results of calculations of recently obtained vibrational distributions of OH formed by water unimolecular dissociation with parameterized collisional energy transfer. The vibrational and rotational state distributions of OH formed as a result of water dissociation have been calculated from the semiclassical molecular dynamics trajectory method. The degree to which the postdissociative nascent distributions will be sustained in the flow depends on the collision rate and will, therefore, be different for 80 and 100 km. The flow conditions corresponding to the BSUV2 are transitional and can only be represented by a rarefied gas technique; hence, the DSMC approach will be used.

The outline of the paper is as follows. The main change to the thermochemical model of earlier work[4] has been the inclusion of state specific OH product distributions obtained from water dissociation. The modeling of unimolecular water dissociation and the resultant product distributions are given in the next section. In the following section, the DSMC method is discussed. Finally, the results of the incorporation of the molecular dynamics dissociation probabilities and product distributions into the DSMC method are presented. The general features of the flowfields will be compared at altitudes from 80 to 100 km at a constant speed of 5 km/s for a 10.16-cm nose radius. Flowfield vibrational and rotational distributions of OH predicted by the molecular dynamics data and the local equilibrium energy redistribution technique will be compared.

II. Modeling of the Unimolecular Dissociation of Water

Molecular dynamics enables one to calculate from first principles probabilities, cross sections, and rate constants for fundamental elementary reaction processes. Because these quantities depend on the motion of the atomic nuclei, a classical rather than exact quantum treatment of that motion has been shown to provide a good approximation for the investigation of reaction mechanisms.[9] The potential energy surface (PES) represents the change in electronic energy as a function of the internuclear distances. When the potential energy surface is obtained using fits to a series of quantum mechanical single energy point calculations, the scattering method is referred to as a semiclassical one. For triatomic molecules, reliable surfaces have been generated using ab initio quantum mechanical calculations as well as experimental data.[10] Such surfaces do not exist, unfortunately, for the water–N_2 interaction. For the collision energies of interest (1.7 eV), the primary method by which the neutral colliders dissociate water is to transfer their kinetic energy to the vibrational modes of water. A classical trajectory calculation of unimolecular water dissociation, that is, water self-dissociation, using an accurate water PES can, therefore, approximate the resultant OH vibrational and rotational product distribution.

Considerable studies have been carried out for the unimolecular dissociation of water.[11–13] These studies, however, have emphasized the product distribution for considerably higher dissociation energies (~9.5 eV) and from the electronically excited states of water and the product distribution of the OH(A) state. Because the energetics of the BSUV2 flows are clearly not this high, the results of earlier unimolecular dissociation studies could not be assumed to be applicable.

A. Method of Calculation

The classical Hamiltonian for the water molecule may be expressed as

$$H = T + V = E \tag{1}$$

For systems of three nuclei and larger, it is most convenient to express the Hamiltonian in the laboratory reference frame in a Cartesian coordinate system. For three nuclei, Hamilton's equations of motion become

$$\dot{p}_{ij} = -\frac{\partial V}{\partial r_{ij}} \tag{2}$$

$$\dot{r}_{ij} = \frac{p_{ij}}{m_i} \tag{3}$$

where the overdot denotes a time derivative, $i = 1, 2, 3$ (atoms), and $j = 1, 2, 3$ (directions). The 18 coupled equations can be solved for the coordinates and momenta of the three-atom system using a fourth-order Runge–Kutta method (see Ref. 14).

The two-valued surface-ground state PES for water calculated by Murrell et al.[15] was used in this work. The use of two diabatic surfaces gives an accurate ground state water PES in the dissociation region, the prime region of interest in our calculations.

Because the trajectory method is deterministic, the 18 initial conditions for the three nuclei must be specified. Specification of initial conditions is more difficult for polyatomic systems, but two possible methods were examined. Shaffer and Newton[16] provide analytic expressions for the normal modes of water in terms of Cartesian coordinate displacements. Initial conditions could be generated using these analytic expressions as follows. The amplitude of each normal mode is proportional to the square root of the vibrational energy of that mode, and the relative phases may be chosen by selecting three random numbers. The normal mode analysis assumes that there are small interatomic displacements, an assumption that is valid for low-energy vibrational states. However, for the flow conditions of interest the deviation of interatomic distances from normal mode behavior can be significant. The second method is more general, does not require a normal mode assumption, and is only dependent on the total internal water energy. The method is based on microcanonical sampling whereby the coordinates and momenta are chosen separately.[17–19] Trajectories are then computed for the set of initial conditions (see Ref. 20 for further details).

The accuracy of the classical trajectory method is governed by a number of numerical issues. In the selection of initial coordinates, a maximum value of 5 Å for the three internuclear distances was selected because it is much larger than the equilibrium internuclear distance of 0.956 Å. The trajectories are computed for a total time of 1×10^{-12} s, which is many vibrational periods. Total energy is conserved to better than 0.005%, and the trajectories are integrated backward in time to return to the initial condition, as a numerical check. Depending on the initial conditions, which govern which portion of the PES will be traversed, the water molecule will either remain intact (not dissociate) or dissociate into OH + H, within the total time of 1×10^{-12} s. The other two reaction channels, O + 2H or H_2 + O, were found to be unlikely for the internal energies of interest here.

B. Calculation of Probability of Dissociation

For any internal energy above the first dissociation threshold, the water molecule will dissociate, given a sufficient length of time, that is,

$$\frac{\mathrm{d}\left[\mathrm{H_2O^*}\right]}{\mathrm{d}t} = -k\left[\mathrm{H_2O^*}\right] \tag{4}$$

where [H_2O^*] is the concentration of internally excited water molecules. The first dissociation threshold is the energy required

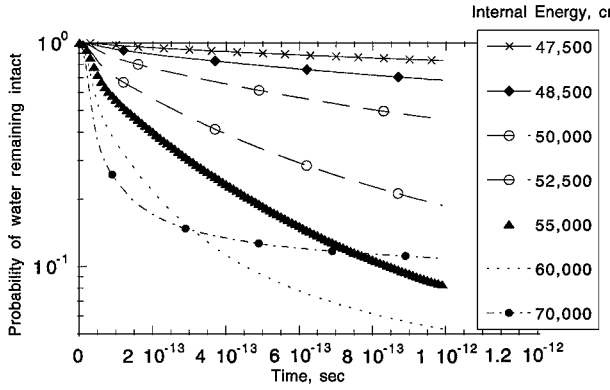

Fig. 1 Reaction probability time dependence as a function of various internal energy values.

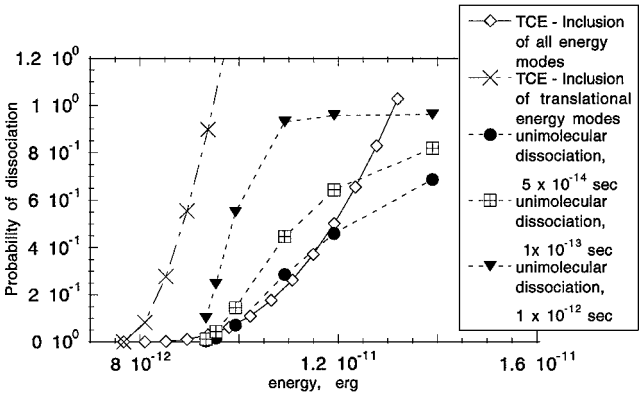

Fig. 2 Comparison of the probability of dissociation as a function of relative collisional energy for the TCE and unimolecular dissociation.

to break the H–OH bond of water and, for the PES used in this work, was approximately 47,500 cm^{-1}. If the reaction dynamics is statistical, the unimolecular decay is governed by a single lifetime. Figure 1 shows a plot of the fraction of water molecules remaining intact as a function of time. Deviation from a straight line (on a log plot) indicates that the reaction dynamics of water dissociation exhibits nonstatistical behavior. Figure 1 shows that the nonstatistical nature increases as the amount of energy above the dissociation barrier is raised. Furthermore, the rate of dissociation increases as the water excitation energy increases. The deviation from statistical unimolecular dissociation has been discussed by Schranz and Sewall[21] and Schranz et al.[22] for other polyatomic systems. Hence it is reasonable that such behavior can be observed for unimolecular water dissociation.

The use of the molecular dynamics unimolecular dissociation to predict a probability of dissociation in the DSMC simulation requires that a specific time constant for water dissociation be chosen. Calculation of the probability of the dissociation of water by a collider would avoid this question because the length of the interaction time would be determined in the context of the scattering calculation and would be a function of the relative collisional velocity and the interaction potential. An approximation to the probability can be made by assuming that the interaction time is the ratio of the effective variable hard-sphere diameter of water and the collider (N_2) to their relative velocity.[23]

Figure 2 shows a comparison of the dissociation rate given by the total collisional energy (TCE)[24] and unimolecular dissociation models. Two extreme conditions are shown for the TCE rate, those where all precollisional energy modes contribute to the reaction process vs the TCE probability when only the precollisional translational energy is included. The energy dependence of the unimolecular rates at various reaction times are also shown. The unimolecular probabilities are seen to have a different energy dependence than the two cases of the TCE model. Moreover, the unimolecular probabilities approach unity as the energy is increased, whereas the TCE model does not. The DSMC simulation results obtained with the TCE model (translational energy only) and the unimolecular dissociation probabilities will be compared in Sec. IV.

C. Final State Distributions

The use of the unimolecular dissociation to predict dissociated product state distributions is the second, and perhaps more important, result of the molecular dynamics approach. For each trajectory, the water is determined to have dissociated if the distance between the H atom and the OH molecule is sufficiently large (larger than 5 Å). The energy after the dissociation is divided into the following components:

$$E = E_{\text{cm}}^{T} + E_{\text{H,OH}}^{T_{\text{rel}}} + E_{\text{OH}}^{T_{\text{rel}}} + V_{\text{OH}} \tag{5}$$

where the sum of the last two terms represents the internal energy of OH if V_{OH} is expressed relative to zero potential energy.

The rotational and vibrational energies of the OH molecule can be described classically, and vibrational and rotation motion are assumed to be separable.[25] At the end of each trajectory (that results in dissociation), the coordinates of OH group are analyzed as a function of time to compute numerically the rotational quantum number J and the vibrational quantum number v (Refs. 20 and 25).

The product distributions of the ensemble of trajectories are used as a database in the DSMC computations. It was found that the distribution of $E_{\text{H,OH}}^{T_{\text{rel}}}$, the relative OH-H translational energy, broadens and shifts to higher translation energy values as the initial water energy increases. Figures 3–5 present examples of the OH product vibrational and rotational quantum number distributions obtained from the molecular dynamics trajectory calculations. The number of trajectories for each initial water energy condition was approximately 50,000. Figure 3 shows the change in vibrational distributions for different water internal energy values. At internal

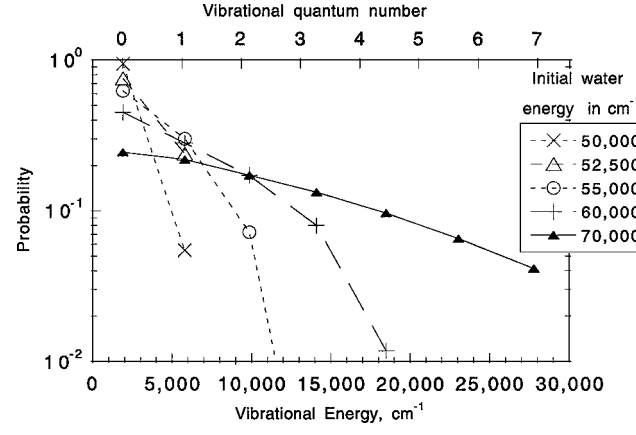

Fig. 3 Comparison of OH vibrational distributions at different water energies.

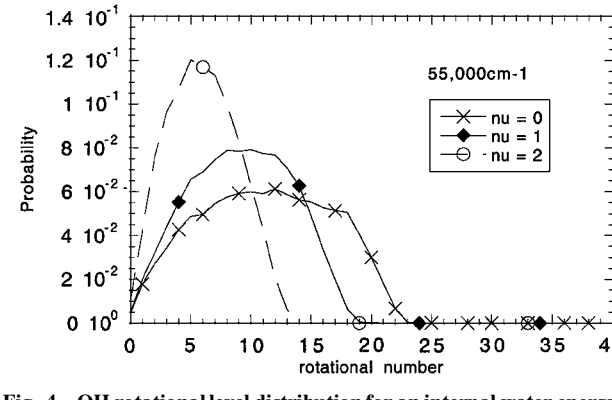

Fig. 4 OH rotational level distribution for an internal water energy of 55,000 cm^{-1}.

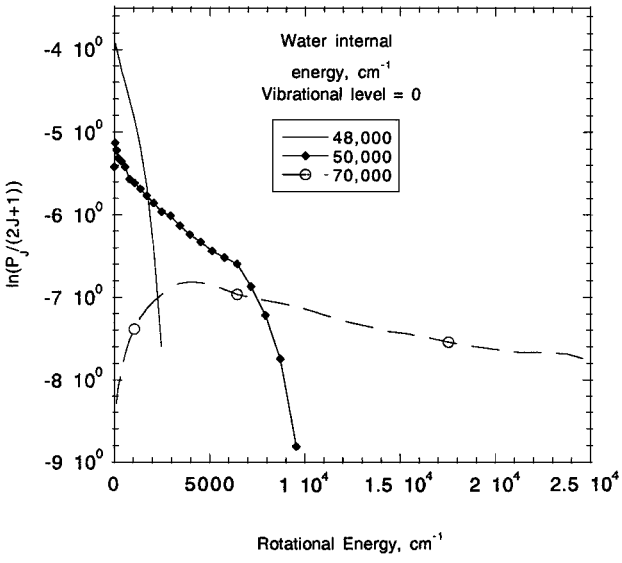

Fig. 5 Comparison of OH rotational level distribution for the 0 vibrational level for different internal water energies.

energies below 50,000 cm^{-1}, there is insufficient energy to populate the $v = 1$ vibrational level, whereas at 70,000 cm^{-1}, the higher levels (up to seventh) are significantly populated. Also as the energy is raised, the effective vibrational temperature increases and the vibrational levels approach a Boltzmann distribution. Figure 4 shows a comparison of the OH rotational distribution at an internal energy of 55,000 cm^{-1} for the first three vibrational levels. There is a maximum in population that shifts to lower rotational quantum number at the higher vibrational quantum number. It was found that as the internal energy was raised the rotational distributions become broader for all vibrational levels. Figure 5 shows a plot of the natural logarithm of the probability of formation in a J level divided by the degeneracy of the level as a function of rotational energy. All curves correspond to the lowest vibrational quantum number for three different water internal energies. Except for the lowest internal energy, it can be seen that the populations deviate strongly from a Boltzmann distribution.

III. Numerical Technique and Collision Models

The SMILE computational tool based on the DSMC method is used in the computations. The details on the method may be found elsewhere.[26] The SMILE capabilities that were used in the present work include models for energy transfer, two-level rectangular grids adaptive to flow gradients, different grids for collisions and macroparameters, and parallel implementation with efficient load balancing techniques. The number of simulated molecules in the computational domain was about 1.3×10^6, a sufficient value to avoid the influence of statistical dependence on the modeling results. Different grids adaptive to flow gradients were used to model collisions and macroparameters. The total number of collision and macroparameter cells was about 150,000 and 30,000, respectively. The total number of time steps was about 50,000 with a timestep of 2×10^{-7} s for 80 km and 2×10^{-6} s for 100 km, and the macroparameter sampling was started after 5000 time steps. Because the residence time of molecules in a collision cell is slightly larger than the time step, and the average number of molecules in a cell is more than 10, the flow parameters presented here are based on an approximate sample size of 10^5 particles. Such a sample size is sufficient to obtain a reasonable accuracy both for macroparameters and distribution functions.

The majorant frequency scheme is employed for modeling molecular collisions.[27] The variable hard sphere model was used for modeling intermolecular interactions. The Larsen–Borgnakke model[28] with temperature-dependent and constant value rotational and vibrational relaxation numbers was utilized for rotation–translation and vibration–translation energy transfer. The TCE model was employed to calculate the cross sections for all gas-phase chemical reactions involving the chemical species N_2 and O_2 and their derivatives. The complete list of N_2 and O_2 reactions may be found in earlier work,[29] and the additional hydrogenated reactions used in this work are given in Table 1.

Table 1 Rate coefficients for hydrogenated reactions

Reaction	Rate coefficient,[a] m^3 molecule^{-1} s^{-1}		
	A	n	E/k_B, K
$H_2O + N_2 \rightarrow OH + H + N_2$	5.81×10^{-15}	0.000	−53,000.0
$H_2O + O_2 \rightarrow OH + H + O_2$	1.13×10^{-7}	−1.31	−59,400.0
$H_2O + O \rightarrow OH + H + O$	1.13×10^{-7}	−1.31	−59,400.0
$OH + N_2 \rightarrow O + H + N_2$	1.25×10^{-15}	0.06	−51,000.0
$OH + O_2 \rightarrow O + H + O_2$	1.25×10^{-15}	0.06	−51,000.0
$OH + O \rightarrow O + H + O$	1.25×10^{-15}	0.06	−51,000.0
$H + O_2 \leftrightarrow OH + O$	3.65×10^{-16}	0.00	−8,450.0
$O + H_2O \leftrightarrow OH + OH$	1.13×10^{-16}	0.00	−9,240.0

[a]Here $k = AT^n \exp(-E/kT)$.

The following procedure is used to model reacting and inelastic processes in the collision routine. The first step after a pair of simulated molecules was accepted for a collision is to check if the pair can undergo chemical reactions. To this end, the probabilities are calculated for all chemical transformations that may occur between the two molecules of given species. For example, in the collision between water and nitrogen molecules, both water and nitrogen may dissociate. (Note that in the TCE model the reaction probability is zero if the collision energy is smaller that the reaction threshold or the dissociation energy.) Then, the appropriate chemical reaction is selected according to the calculated probabilities. After the reaction path is chosen, the total energy available is reduced to account for the reaction heat or dissociation energy and is distributed over the energy modes of reaction products. (The energy redistribution mechanisms are given subsequently.) If no reaction occurred, the collision pair is checked for the possibility of the energy exchange between the translational and internal modes (inelastic collisions). The probability of an inelastic collision is inversely proportional to the rotational and vibrational relaxation numbers Z_r and Z_v. The detailed modeling of collisions that involve internal energy transfer is more complicated for polyatomic systems and will be the subject of future work. Here we present results using the temperature-dependent variable Z_r and Z_v model.

The first three reactions of Table 1, the dissociation of water, are the important mechanisms of OH production in these flows. The Arrhenius data related to the first three reactions from Table 1 were used to calculate the water dissociation cross sections based on the TCE model. The OH and H_2O species were considered as trace species whose weighting factor was varied from 10^{-5} to 10^{-9} depending on the altitude of the simulation. The species weighting scheme[29,30] was utilized in the computations. The reaction cross sections were also calculated using molecular dynamics calculations of unimolecular dissociation (UD) in the manner discussed in Sec. II.B. The use of a reaction cross section derived from unimolecular rates requires an assessment of the degree of conversion of translational energy into internal water energy, before the water self-dissociates. This conversion efficiency η was parameterized with values of 10–100%. The choice of η affects the selection of dissociation probability values used to assess the outcome of the collision, that is, the choice of the abscissa of Fig. 2, as well as the energy that will be available for OH final state product redistribution, that is, which curve to select from Fig. 3.

Two energy redistribution models were considered. The baseline model for energy redistribution was that suggested by Haas.[31] The details of the first energy redistribution model are as follows. First, the total collision energy E_c is calculated. The total collision energy is the sum of the relative translational and internal energies of the reactants. Then, all reactant species energies (relative translational, rotational, and vibrational) are multiplied by a factor of $(E_c - E_d)/E_c$, where E_d is the water dissociation threshold. The new velocities of H_2O and the collision partner are calculated. Afterward, the water molecule is divided into OH and H. The energies

of the OH–H pair (relative translational OH internal energies) are calculated so that the magnitude is proportional to the number of degrees of freedom of the corresponding modes and the sum is equal to the sum of rotational and vibrational energies of water. Finally, new velocities of OH and H are calculated using new relative translational energy of the OH–H pair and the velocity of the center of mass equal to the water velocity.

The algorithm for energy redistribution for the $H_2O + M \rightarrow OH + H + M$ dissociation reaction may be represented by the following three main steps:

1) The energy of reaction is calculated,

$$E_c = E_{\text{trn},H_2O-M} + E_{\text{int},H_2O}$$

2) The dissociation energy E_d is proportionally subtracted from the energy modes that contribute to dissociation as follows:

$$E'_c = E_c - E_d = E'_{\text{trn},H_2O-M} + E'_{\text{int},H_2O}$$

$$= E_{\text{trn},H_2O-M}[(E_c - E_d)/E_c)] + E_{\text{int},H_2O}[(E_c - E_d)/E_c]$$

where the prime denotes the properties after the dissociation energy subtraction.

3) The final postreaction energies are calculated

$$E''_{\text{trn,OH-H}} = \frac{\xi_{\text{trn,OH-H}}}{\xi_{\text{trn,OH-H}} + \xi_{\text{int,OH}}} E'_{\text{int},H_2O}$$

$$E''_{\text{rot,OH}} = \frac{\xi_{\text{rot,OH}}}{\xi_{\text{trn,OH-H}} + \xi_{\text{int,OH}}} E'_{\text{int},H_2O}$$

$$E''_{\text{vib,OH}} = \frac{\xi_{\text{vib,OH}}}{\xi_{\text{trn,OH-H}} + \xi_{\text{int,OH}}} E'_{\text{int},H_2O}$$

With such a redistribution, the internal energies of OH are proportional to the internal energy E_{int,H_2O} of H_2O.

The second energy redistribution model utilizes the rotational and vibrational OH product distributions obtained from the molecular dynamics calculations presented in Sec. II.C. Once again, this redistribution will depend on the conversion efficiency of translational collisional energy to internal water energy, and results will be presented for the two limiting cases of $\eta = 10$ and 100%.

The gas–surface interaction was modeled using the Maxwell model. Three different accommodation coefficients were utilized for translational, rotational, and vibrational modes of reflected molecules. A value of the translational accommodation coefficient of 0.85 was assumed, whereas a smaller value of 0.5 was used for the internal energy accommodation coefficients. For high-energy collisions simulated in this work, the internal energy accommodation coefficients may be even lower.[32]

IV. Results

The results include a discussion of the general properties of the flowfield and a description of the resulting OH vibrational distributions. The results are presented for altitudes 80 and 100 km using three chemistry/energy redistribution models. The baseline model is the TCE chemistry model with the energy redistribution calculated according to Haas[31] model (HM). In the second model, water dissociation probabilities obtained from the unimolecular dissociation calculations are used and HM is utilized for energy redistribution. Finally, the third model utilizes the unimolecular probabilities with the unimolecular OH product distribution results. Table 2 summarizes the nature of these three models.

A. General Flowfield Features

In this subsection, we discuss the macroscopic parameters of the flow. Note that the chemistry model does not impact the properties of major flow species N_2, O_2, and O. Table 3 gives the freestream conditions for the two altitudes for which results will be shown. Figure 6 shows the total number densities contours for 80 and 100 km. Figure 6 shows the growth of the shock layer width as the rarefaction increases. Figure 7 shows the corresponding translational

Table 2 Flowfield water dissociation chemistry models

Model description	Water dissociation probability	Energy redistribution model
Baseline TCE-HM	Total collisional energy	Haas model
Model 1 UD-HM	Unimolecular dissociation	Haas model
Model 2 UD-MD, $\eta = 10, 100\%$	Unimolecular dissociation	Molecular dynamics

Table 3 Freestream conditions

Altitude, km	Total number density, number/m^3	Water mole fraction	OH mole fraction	Temperature, K
80	4.18×10^{20}	5.6×10^{-6}	4.3×10^{-9}	181
100	1.19×10^{19}	7.2×10^{-7}	2.0×10^{-10}	185

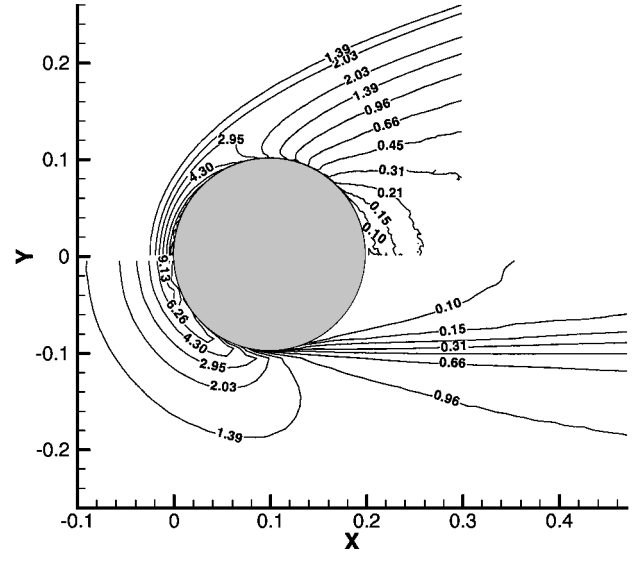

Fig. 6 Comparison of total number densities normalized by freestream values for 80 km (top) and 100 km (bottom).

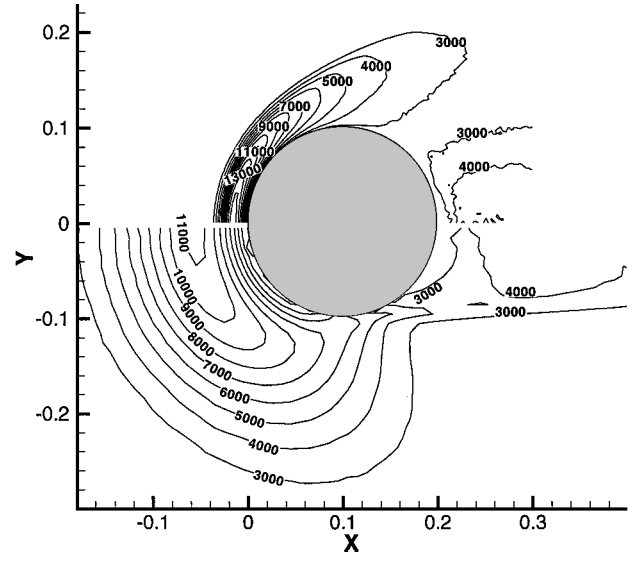

Fig. 7 Comparison of translational temperature (K) for 80 km (top) and 100 km (bottom).

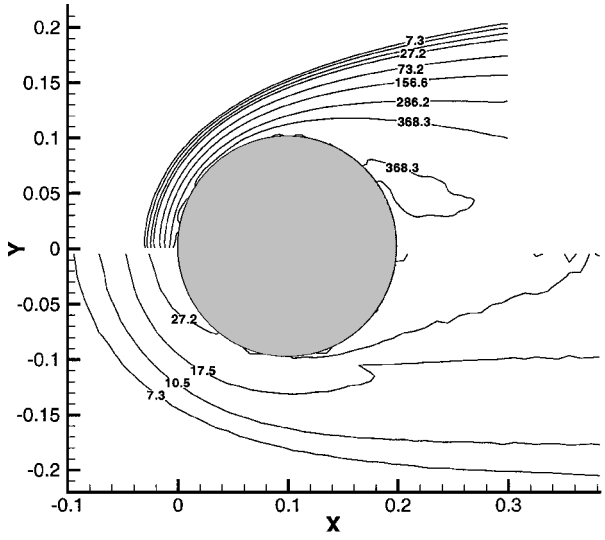

Fig. 8 Comparison of OH number density normalized by the freestream value for 80 km (top) and 100 km (bottom); TCE-HM model.

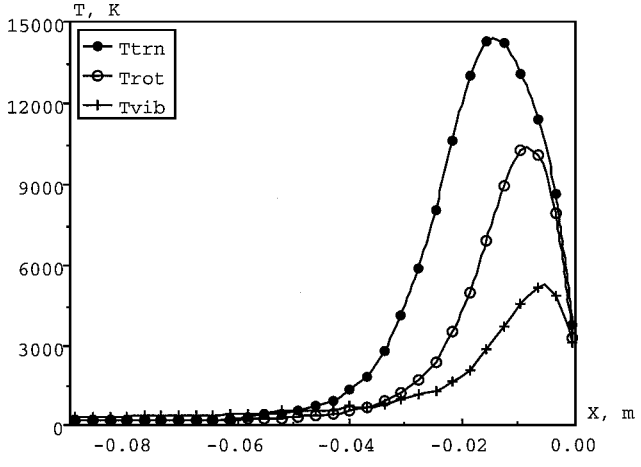

Fig. 9 N_2 temperature profiles along the stagnation streamline for 80 km.

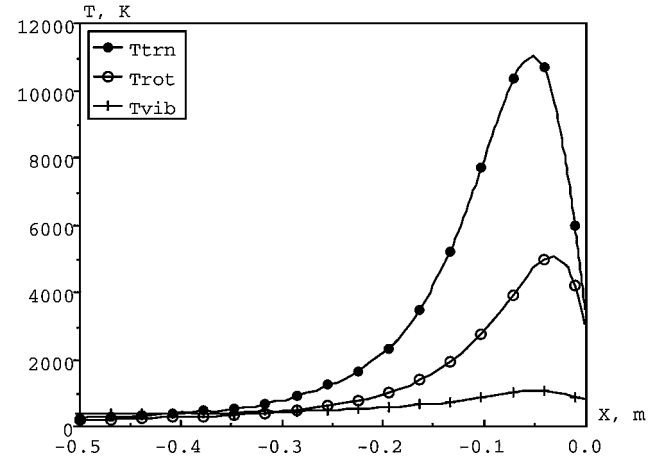

Fig. 10 N_2 temperature profiles along the stagnation streamline for 100 km.

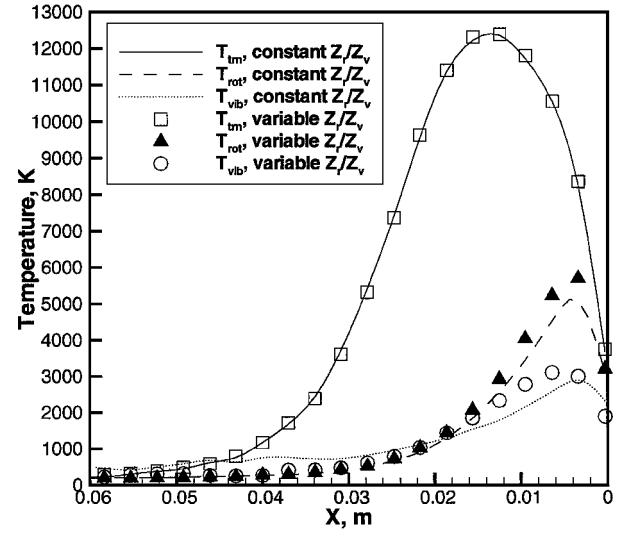

Fig. 11 Comparison of water internal temperature profiles along the stagnation streamline for 80 km calculated using the variable and constant rotational and vibrational excitation models.

temperature contours for 80- and 100-km altitudes. The maximum translational temperatures at both altitudes and approximately the same, with a somewhat higher value at 80 km. To illustrate the difference in water dissociation rates for the two altitudes considered, Fig. 8 compares the spatial distributions of OH number density for 80- and 100-km altitudes. The freestream number densities of OH at 80 and 100 km are 1.8×10^{12} and 2.4×10^{9} m, respectively. The baseline chemistry model was used in these computations. The structure of the fields is qualitatively similar to that of the bulk shown in Fig. 6, with the peak value at 80 km a factor of $\sim 1.25 \times 10^{4}$ higher than that at 100 km. Approximately three orders of magnitude in the peak ratio is due to the change in freestream OH concentration, and one order of magnitude is due to the slower rate of water dissociation.

The difference in the bulk translational, rotational, and vibrational temperature for the two altitudes under consideration can be seen in closer detail by examining the spatial distribution along the stagnation streamline. Figures 9 and 10 show that the flow exhibits thermal nonequilibrium both for 100 and 80 km. All temperatures are higher at 80 km than the respective values at 100 km. The reduction in the bulk translational temperature, as well as number density, at 100 km indicates that the relative collision velocities will be lower, and hence, the water dissociation rate will be reduced for all of the three chemical models considered here.

The amount of OH formed as well as its final state vibrational distribution will depend on the characteristics of the water molecules in the flow. Figure 11 shows a comparison of the water translational, rotational, and vibrational temperatures along the stagnation streamline at 80-km altitude for the baseline chemistry model with constant as well as temperature-dependent rotational and vibrational collision numbers Z_v and Z_r. For reference, Fig. 12 shows the values of the collision numbers along the stagnation streamline at 80 km for the temperature-dependent model. Constant numbers of $Z_r = 5$ and $Z_v = 250$ were used for the model with constant collision numbers.[33] All three vibrational modes were modeled as separate states for water. The vibrational temperature represents an average over the three vibrational modes. Figure 12 shows that even at 80 km there is a high degree of nonequilibrium between the internal (vibrational and rotational) and translational energy modes. Figure 11 shows that there is no significant difference between the two models of energy transfer. Obviously at 100 km the collision rate is lower, and the difference between the water temperatures for the two collision models is even smaller than at 80 km. Hence, the following OH results are all based on the temperature-dependent energy transfer model.

B. Sensitivity to Water Chemistry Modeling

In this subsection, we consider the sensitivity of the OH concentrations and temperatures to the water dissociation models given in Table 2. The variation of these characteristics with respect to the water dissociation model and altitude could result in important changes in the OH UV spectra.

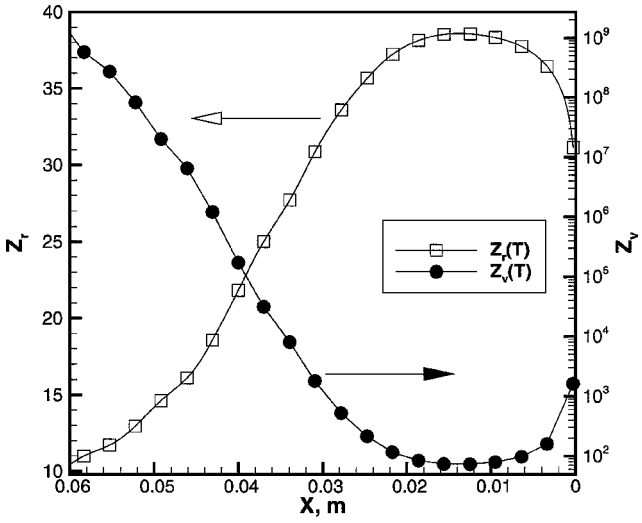

Fig. 12 Rotational and vibration relaxation numbers as a function of distance along the stagnation streamline at 80 km for the variable-temperature relaxation models.

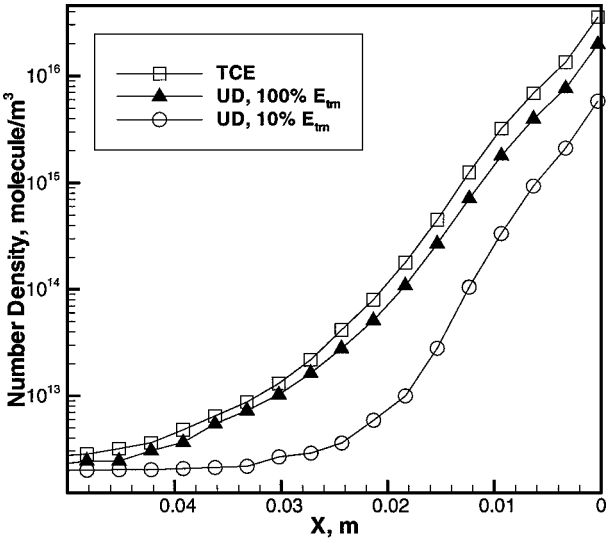

Fig. 13 Comparison of OH number density profiles along the stagnation streamline at 80 km for the TCE-HM and UD-HM models with different energy contributions.

Consider the sensitivity of OH production to the reaction probability model, that is, TCE-HM and UD-HM. Figures 13 and 14 show OH number density at 80 and 100 km for these two models. In Figs. 13 and 14 the body is located at $X = 0$. The different slope of the reaction probabilities as a function of collision energy for the two models discussed in the preceding sections causes a difference in the slope for the TCE model and the UD model with $\eta = 100\%$ (Fig. 13). Generally, the UD model predicts a lower OH density in the shallow portion of the shock and slightly higher values closer to the wall. The UD model with $\eta = 10\%$ shows a significant delay in producing OH connected to a certain induction time necessary to excite rotational and vibrational modes of water molecules. Similar differences in terms of dissociation incubation were observed by other workers for air species N_2 and O_2 when the TCE model was compared with models that account for vibration–dissociation coupling.[34,35] This behavior is even more pronounced at 100 km, where a smaller degree of water internal mode excitation is observed. Note the distribution function of energy of reacting molecules is narrower for 100 km, and a small difference between the TCE model and the UD model with $\eta = 100\%$ shows that the difference in reaction probabilities is small for this range of collision energies. Similar to an altitude of 80 km, the UD model produces higher values closer to the wall.

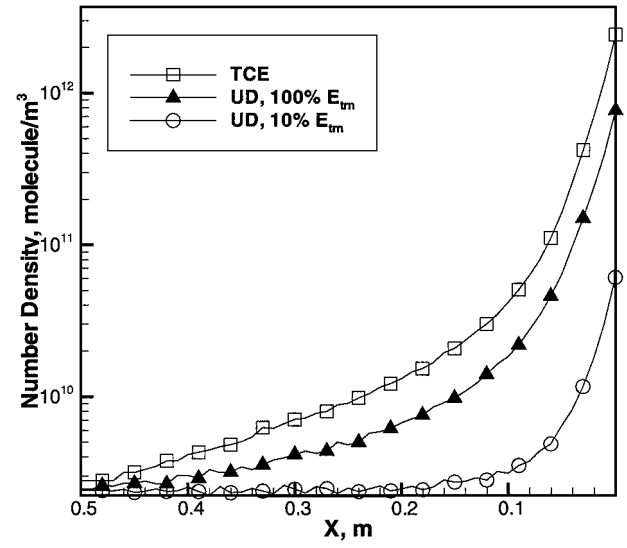

Fig. 14 Comparison of OH number density profiles along the stagnation streamline at 100 km for the TCE-HM and UD-HM models with different energy contributions.

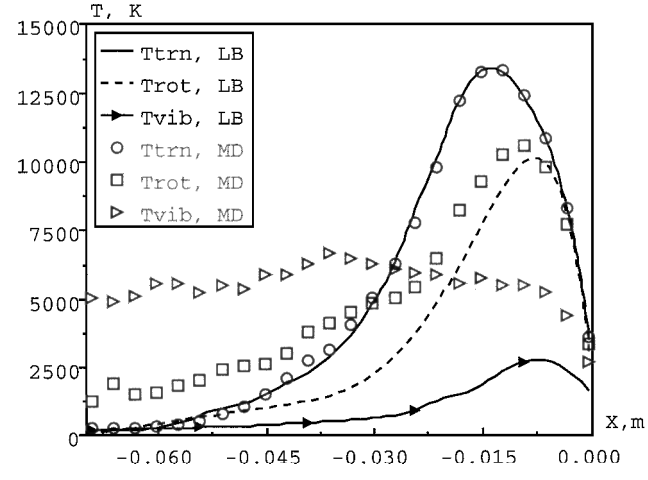

Fig. 15 OH temperature profiles along the stagnation streamline at 80 km for the UD-HM energy redistribution model.

Let us now compare the temperatures of OH for different water dissociation models. The OH temperature profiles depend both on altitude and the manner of energy redistribution. The first dependence comes from the impact of the collision rate on the water internal energy distribution. To analyze the second dependence, the comparison is shown for the UD-HM and UD-molecular dynamics (MD) models, with two values of precollisional energy contribution (the OH temperatures obtained from the TCE model were found to be identical to those of the UD-HM model). The OH temperature profiles obtained by these two water chemistry models were found to be considerably different.

Figure 15 shows a comparison of the OH translational, rotational, and vibrational temperatures along the stagnation streamline at 80 km for the HM model of energy redistribution. Similar to the water temperatures, the three OH modes are in thermal nonequilibrium, and the peak OH vibrational temperature of approximately 3000 K is lower than both the rotational and translational temperatures. Figure 16 shows a comparison of the OH temperature profiles along the stagnation streamline at 80 km for different energy contributions to the MD energy redistribution. Comparison of Figs. 15 and 16 shows that the OH translational temperature profiles are very close for the HM and UD models with $\eta = 100\%$, but the OH rotational and vibrational temperatures have a different spatial distribution. In the region where the rotational temperature reaches a maximum, both models give similar results, but the HM

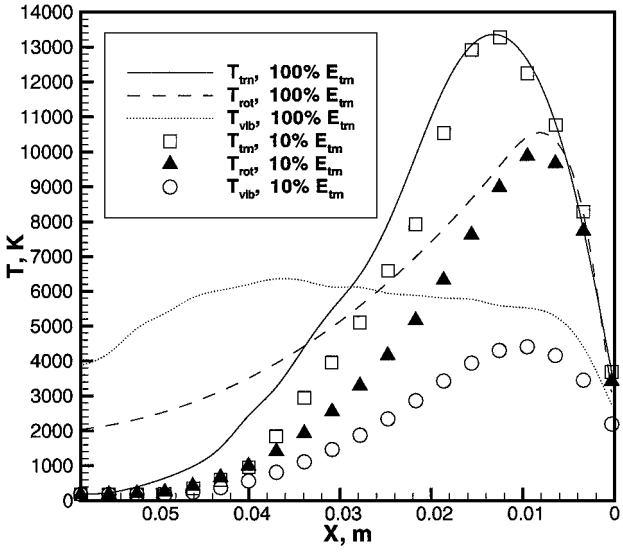

Fig. 16 Comparison of OH temperature profiles along the stagnation streamline at 80 km for different energy contributions to the UD-MD energy redistribution model.

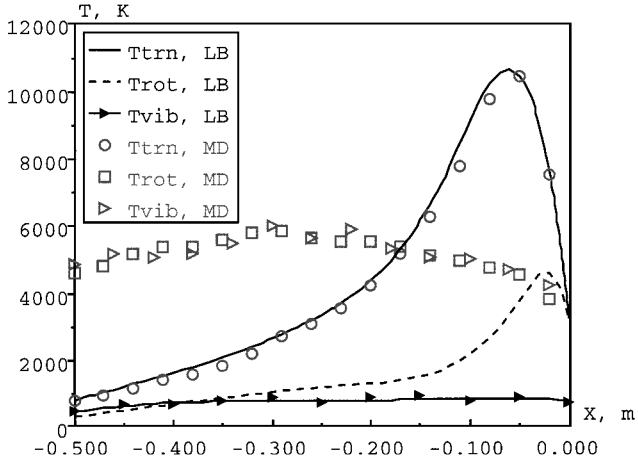

Fig. 17 OH temperature profiles along the stagnation streamline at 100 km for the UD-HM energy redistribution model.

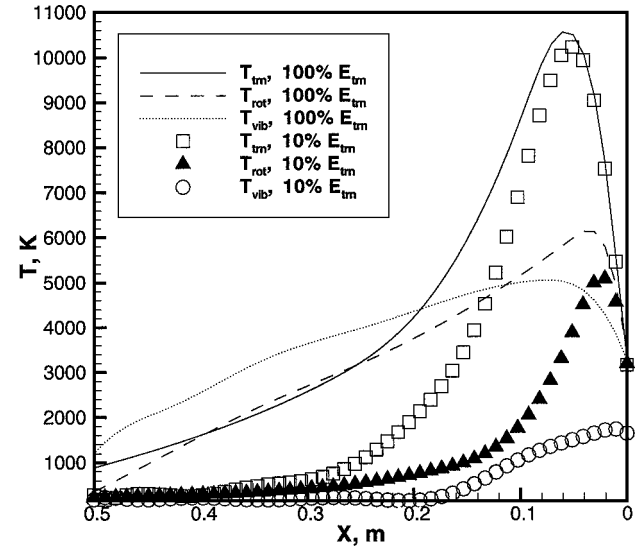

Fig. 18 Comparison of OH temperature profiles along the stagnation streamline at 100 km for different energy contributions to the UD-MD energy redistribution model.

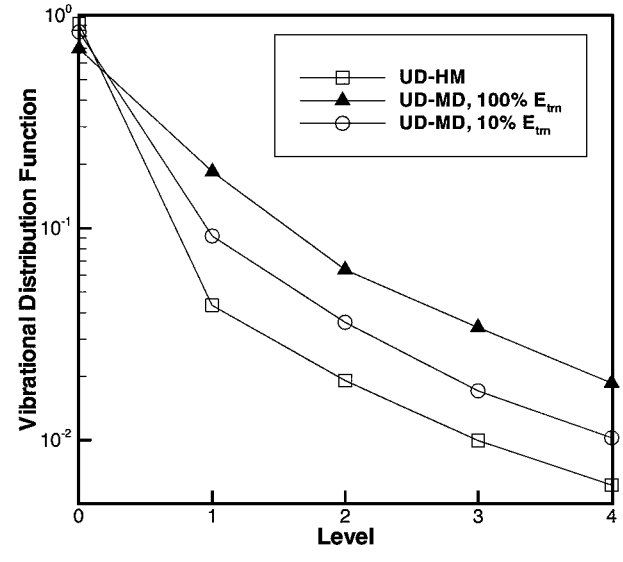

Fig. 19 Comparison of OH vibrational distributions at 80 km for different methods of energy redistribution (UD-HM vs UD-MD) models; $X = -0.009$ m, $Y = 0$.

model predicts lower rotational temperatures than MD. Figure 16 shows that the degree of precollisional translational energy contribution does not significantly effect the translational and rotational temperatures. Comparison of Figs. 15 and 16 also shows that the OH vibrational temperatures are substantially different in terms of magnitudes and shapes for both distribution models and the degree of precollisional translational energy contribution. In Figs. 15 and 16, the body is located at $X = 0$. With $\eta = 10\%$, the shape of the OH vibrational temperature along the stagnation streamline is similar to that predicted by the UD-HM model; however, the maximum OH vibrational temperature is greater by 1000 K.

Figures 17 and 18 show the effect of a lower collision rate. In Figs. 17 and 18, the body is located at $X = 0$. Similar to the 80-km predictions, only the OH translational temperature profiles are the same for both methods of energy redistribution and η. The number of collisions in the flow is so small at 100 km that both the rotational and vibrational temperatures obtained by the HM energy redistribution procedure are found to be significantly lower than those obtained with the molecular dynamics if 100% contribution of translational precollisional energy is assumed. The OH rotational temperature given by the UD-MD model with $\eta = 10\%$ has a distribution along the stagnation streamline similar to that of the UD-HM redistribution model and a slightly larger magnitude. The magnitude of the OH vibrational temperature and its distribution along the stagnation streamline are found to be very different for the three energy redistribution models.

C. OH Vibrational Distributions

The OH temperature profiles given in the preceding section demonstrate nonequilibrium among translational, rotational, and vibrational modes within the shock front, but to understand the BSUV2 spectra we are especially interested in the vibrational distibution of OH at selected locations along the stagnation streamline. By examining the discrete OH vibrational populations at selected points along the stagnation streamline, we can ascertain the true degree of vibrational nonequilibrium and the $v = 0, 1$ populations for the three distribution models. The $v = 0, 1$ populations are of interest because they relate to the BSUV2 high altitude OH spectra. In previous work,[7] we showed that the spectra could only be modeled if one assigned vibrational and rotational temperatures that were considerably different from that of the bulk (N_2) flow. The OH UV spectral peak height ratio at 280 nm (the 1–0 band) and the 310 nm (the 0–0 band) are dependent mainly on the vibrational temperature.

Figure 19 shows a comparison of the OH vibrational distributions at 80 km for different methods of energy redistribution at

$X = -0.009$ m, $Y = 0$. This corresponds to the point along the stagnation streamline where the OH vibrational temperature predicted by the UD-HM redistribution model is highest (Fig. 15). The coordinate $X = 0$ corresponds to the position of the surface. Figure 19 shows that for the lowest altitude considered here, none of the redistribution models gives an equilibrium distribution of vibrational states. The UD-MD model gives a lower 0–1 vibrational state ratio than the UD-HM model. As expected, the ratio of 0–1 vibrational populations is reduced if a higher percentage of precollisional translational energy is assumed. This is because more energy is transferred to the water internal modes and, therefore, available to populate the higher OH vibrational states. The UD-MD with $\eta = 100\%$ would overpredict the ratio of the spectral features, and the $\eta = 10\%$ would underpredict it. The UD-HM model would predict no noticeable radiation peak corresponding to the $1 \rightarrow 0$ transition.

A similar comparison of the three OH vibrational state distributions for 100 km at $X = -0.015$ m along the stagnation streamline is shown in Fig. 20. The location in the flow chosen corresponds to that where the UD-HM model predicted an OH vibrational temperature of ~900 K and the UD-MD with $\eta = 100$ and 10% contribution predicted OH vibrational temperatures of 4500 and 1700 K,

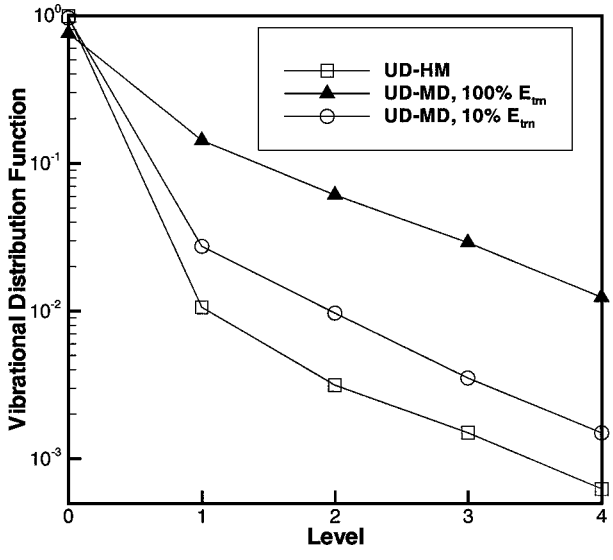

Fig. 20 Comparison of OH vibrational distributions at 100 km for different methods of energy redistribution (UD-HM vs UD-MD) models; $X = -0.015$ m, $Y = 0$.

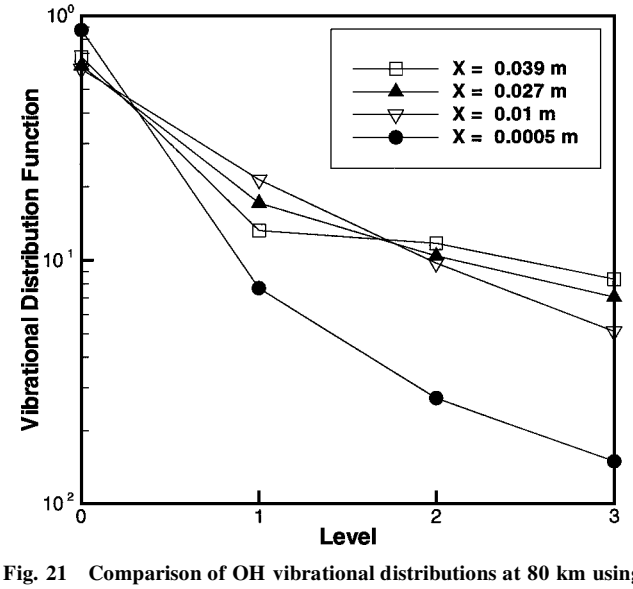

Fig. 21 Comparison of OH vibrational distributions at 80 km using the UD-MD model with 100% contribution of translational energy for different locations along the stagnation streamline, $Y = 0$.

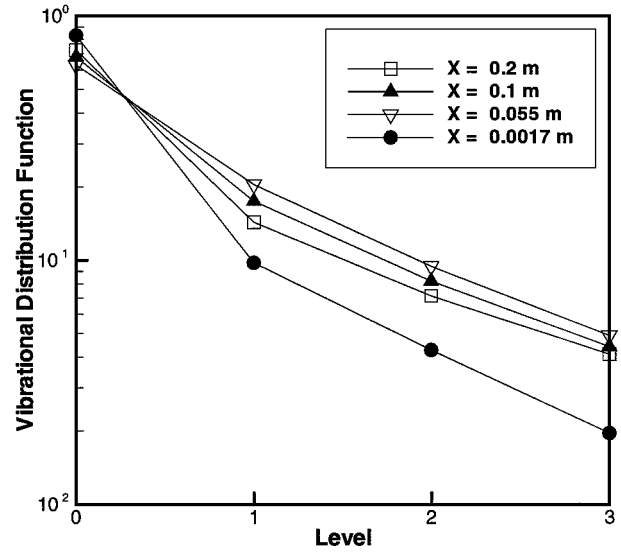

Fig. 22 Comparison of OH vibrational distributions at 100 km using the UD-MD model with 100% contribution of translational energy for different locations along the stagnation streamline, $Y = 0$.

respectively. None of the energy redistribution models predict an equilibrium vibrational distribution, although levels 1–4 approach an equilibrium distribution. Collisions with the cold wall provide the main source for deviation from an equilibrium distribution for the 0 and 1 vibrational states. Only the UD-MD model with $\eta = 100\%$ gives a peak ratio close to experiment.

Figures 21 and 22 show comparisons of the OH vibrational distributions at different locations along the stagnation streamlines for the 80- and 100-km cases, respectively. For all locations, at both altitudes, all of the OH distributions are nonequilibrium. For the point closest to the wall (value closest to zero) the ratio between the zeroth and first vibrational states populations is highest, indicating the influence of gas molecules colliding with a cooler wall. Moving away from the wall toward the peak of the shock, the 0–1 state ratio will decrease. As we proceed toward the freestream, where the gas translational temperatures will be lower, the first vibrational state population starts to decrease again. The difference in the distribution shape for 80 and 100 km is due to the significant impact of collisional relaxation in the shock front at 80 km.

V. Conclusions

A semiclassical molecular dynamics approach has been used to model the dissociation of water to form the hydroxyl radical. The unimolecular dissociation of water is used to model the probability of reaction, as well as to determine the product OH translational, vibrational, and rotational energy distributions. These data have been incorporated into the DSMC method to predict OH concentrations in the flow and OH vibrational state distributions. The use of a semiclassical molecular dynamics approach requires an accurate scattering potential, which is not readily available for all molecular systems. When such surfaces can be calculated by quantum chemistry techniques, the molecular dynamics approach avoids assumptions related to energy redistributions among different energy modes that must be made for other DSMC chemistry models.

Specifically, we note that the unimolecular water dissociation rates are similar to those predicted by the conventional TCE model for this reaction if it is assumed that all of the precollisional translational energy contributes to the dissociation reaction. However, if the contribution is set to a more realistic value of 10% (approximate amount of energy transferred between translational and internal energies on average during the collision), the rates are considerably lower for the unimolecular dissociation model.

When we compare the product distributions obtained from the trajectory calculations with those derived from the equipartition (HM) DSMC model we find that the distributions are significantly

different. The molecular dynamics tends to predict a greater population of the higher OH vibrational states. None of the redistribution models, however, predict an equilibrium OH vibrational distribution. As the flow rarefaction increases, the differences between the two redistribution techniques and the degree of precollisional translational energy contribution becomes more important. The variation among the three models suggests that a more detailed treatment where the full collision can be modeled is necessary.

Acknowledgments

The work was supported by the Army Research Office Grant DAAG55-98-1-009, the Air Force Office of Scientific Research Grant F49620-99-1-0143, and the Ballistic Missile Defense Organization.

References

[1]Levin, D., Collins, R., Candler, G., Wright, M., and Erdman, P., "Examination of OH Ultraviolet Radiation from Shock-Heated Air," *Journal of Thermophysics and Heat Transfer*, Vol. 10, No. 2, 1996, pp. 200–208.

[2]Bose, D., and Candler, G. V., "Thermal Rate Constants of the $N_2 + O \rightarrow NO + N$ Reaction Using *ab initio* $3A''$ and $3A^1$ Potential Energy Surfaces," *Journal of Chemical Physics*, Vol. 104, No. 8, 1996, pp. 2825–2833.

[3]Boyd, I. D., Bose, D., and Candler, G. V., "Monte Carlo Modeling of Nitric Oxide Formation Based on Quasiclassical Trajectory Calculations," *Physics of Fluids*, Vol. 9, No. 4, 1997, pp. 1162–1170.

[4]Gimelshein, S., Levin, D., and Collins, R., "Modeling of Infrared Radiation in a Space Transportation System Environment," AIAA Paper 2000-0731, Jan. 2000.

[5]Baulch, D. L., Drysdale, D. D., Home, D. G., and Lloyd, A. C., *Evaluated Kinetic Data for High Temperature Reactions, Vol. 1, Homogeneous Gas Phase Reactions of the H_2–O_2 System*, Butterworths, London, 1972.

[6]Copeland, R. A., Wise, M. L., and Crosley, D. R., "Vibrational Energy Transfer and Quenching of OH ($A^2\,\Sigma^+$, $V' = 1$)," *Journal of Physical Chemistry*, Vol. 92, No. 20, 1988, pp. 5710–5715.

[7]Levin, D., Laux, C., and Kruger, C., "A General Model for the Spectral Calculation of OH Radiation in the Ultraviolet," *Journal of Quantitative Spectroscopy and Radiative Transport*, Vol. 61, No. 3, 1999, pp. 377–392.

[8]Kossi, K. K., and Boyd, I. D., "Detailed Computation of Ultraviolet Spectra in Rarefied Hypersonic Flow," *Journal of Spacecraft and Rockets,* Vol. 35, No. 5, 1998, pp. 653–659.

[9]Billing, G. D., and Mikkelsen, K. V., *Introduction to Molecular Dynamics and Chemical Kinetics*, Wiley, New York, 1996.

[10]Murrell, J. H., Carter, S., Farantos, S. C., Huxley, P., and Varandas, A. J. C., *Molecular Potential Energy Functions*, Wiley, New York, 1984.

[11]Schinke, R., *Photodissociation Dynamics: Spectroscopy and Fragmentation of Small Polyatomic Molecules*, Cambridge Univ. Press, Cambridge, England, U.K., 1993.

[12]Nyman, G., Ryenfors, K., and Holmlid, L., "Energy Distributions from Decomposition of a Complex $H_2O \rightarrow OH + H$ on a Simplified Potential Energy Surface, as a Function of Total Angular Momentum: Comparison Between Classical Trajectories and an RRKM-Type Statistical Simulation," *Chemical Physics*, Vol. 134, No. 2–3, 1989, pp. 355–373.

[13]Guo, H., and Murrell, J. N., "A Classical Trajectory Study of the $\tilde{A}$-State Photodissociation of the Water Molecule," *Journal of the Chemical Society, Faraday Transactions 2*, Vol. 84, No. 7, 1988, pp. 949–959.

[14]Abramowitz, M., and Stegun, I. A., *Handbook of Mathematical Functions, with Formulas, Graphs, and Mathematical Tables*, Dover, New York, 1970.

[15]Murrell, J. N., Carter, S., Mills, I. M., and Guest, M. F., "Analytical Potentials for Triatomic Molecules VIII. A Two-Valued Surface for the Lowest $1A'$ States of H_2O," *Molecular Physics*, Vol. 42, No. 3, 1981, pp. 605–627.

[16]Shaffer, W. H., and Newton, R. R., "Valence and Central Forces in Bent Symmetrical XY_2 Molecules," *Journal of Chemical Physics,* Vol. 10, No. 7, 1942, pp. 405–409.

[17]Nyman, G., Rynefors, K., and Holmlid, L., "Efficient Microcanonical Sampling for Triatomic Molecular Systems: Exact Distributions Verified," *Journal of Chemical Physics*, Vol. 88, No. 6, 1986, pp. 3571–3580.

[18]Nyman, G., Nordholm, S., and Schranz, H. W., "Efficient Microcanonical Sampling for a Preselected Total Angular Momentum," *Journal of Chemical Physics,* Vol. 93, No. 9, 1990, pp. 6767–6773.

[19]Severin, E. S., Freasier, B. C., Hamer, N. D., Jolly, D. L., and Nordholm, S., "An Efficient Microcanonical Sampling Method," *Chemical Physics Letters*, Vol. 57, No. 1, 1978, pp. 117–120.

[20]Levin, D. A., and Gimelshein, S. F., "Modeling of OH Vibrational Distributions Using Molecular Dynamics with the Direct Simulation Monte Carlo Method," AIAA Paper 2000-2432, June 2000.

[21]Schranz, H. W., and Sewall, T. D., "Statistical and Dynamical Behavior in the Unimolecular Reaction Dynamics of Polyatomic Molecules," *Journal of Molecular Structure: THEOCHEM*, Vol. 368, No. 1–3, 1996, pp. 125–131.

[22]Schranz, H. W., Raff, L. M., and Thompson, D. L., "Intramolecular Energy Transfer and Mode-Specific Effects in Unimolecular Reactions of Disilane," *Journal of Chemical Physics*, Vol. 95, No. 1, 1991, pp. 106–120.

[23]Levine, R. D., and Bernstein, R. B., *Molecular Reaction Dynamics*, Oxford Univ. Press (Clarendon), London, 1987.

[24]Bird, G. A., "Monte Carlo Simulation in an Engineering Context," *Rarefied Gas Dynamics*, edited by S. Fisher, Vol. 74, Progress in Astronautics and Aeronautics, AIAA, New York, 1981, pp. 239–255.

[25]Porter, R. N., and Raff, L. M., "Classical Trajectory Methods in Molecular Collisions," *Dynamics of Molecular Collisions*, Pt. B, edited by W. H. Miller, Plenum, New York, 1976, pp. 1–52.

[26]Ivanov, M. S., Markelov, G. N., and Gimelshein, S. F., "Statistical Simulation of Reactive Rarefied Flows: Numerical Approach and Applications," AIAA Paper 98-2669, June 1998.

[27]Ivanov, M. S., and Rogasinsky, S. V., "Analysis of the Numerical Techniques of the Direct Simulation Monte Carlo Method in the Carefied Gas Dynamics," *Soviet Journal of Numerical and Analytical Mathematical Modeling*, Vol. 3, No. 6, 1988, pp. 453–465.

[28]Borgnakke, C., and Larsen, P. S., "Statistical Collision Model for Monte Carlo Simulation of Polyatomic Gas Mixture," *Journal of Computational Physics*, Vol. 18, No. 4, 1975, pp. 405–420.

[29]Gimelshein, S. F., Levin, D. A., and Collins, R. J., "Modeling of Glow Radiation in the Rarefied Flows about an Orbiting Spacecraft," *Journal of Thermophysics and Heat Transfer*, Vol. 14, No. 4, 2000, pp. 471–479.

[30]Bird, G. A., *Molecular Gas Dynamics and the Direct Simulation of Gas Flows*, Clarendon, Oxford, England, U.K., 1994.

[31]Haas, B. L., "Models of Energy Exchange Mechanics Applicable to a Particle Simulation of Reactive Flow," *Journal of Thermophysics and Heat Transfer*, Vol. 6, No. 2, 1992, pp. 200–212.

[32]Boyd, I., Phillips, W., and Levin, D., "Prediction of Ultraviolet Radiation in Nonequilibrium Hypersonic Bow-Shock Waves," *Journal of Thermophysics and Heat Transfer*, Vol. 12, No. 1, 1998, pp. 38–44.

[33]Dunn, M. G., Skinner, G. T., and Treanor, C. E., "Infrared Radiation from H_2O, CO_2, or NH_3 Collisionally Exited by N_2, O, or Ar," *AIAA Journal*, Vol. 13, No. 6, 1973, pp. 803–812.

[34]Boyd, I. D., "Analysis of Vibration–Dissociation–Recombination Processes Behind Strong Shock Waves of Nitrogen," *Physics of Fluids A*, Vol. 4, No. 1, 1992, pp. 178–185.

[35]Haas, B. L., and Boyd, I. D., "Models for Direct Monte Carlo Simulation of Coupled Vibration–Dissociation," *Physics of Fluids A*, Vol. 5, No. 2, 1993, pp. 478–489.